Understanding the high-resolution spectral signatures of Ar-D_2O in the 3OD stretch region measured by cavity ringdown absorption spectroscopy

R. Glorieux,[a] A. S. Bogomolov,[a] M. Herman,[b] N. Moazzen-Ahmadi,[c] A. R. W. McKellar,[d] C. Lauzin[a]

[a] *Institute of Condensed Matter and Nanosciences, Université catholique de Louvain (UCLouvain), Chemin du cyclotron 2, Louvain-la-Neuve, 1348, Belgium*

[b] *Spectroscopy, Quantum Chemistry and Atmospheric Remote Sensing (SQUARES), Faculté des Sciences, Université libre de Bruxelles (ULB), 50 ave. F-D Roosevelt, Brussels, 1050, Belgium*

[c] *Department of Physics and Astronomy, University of Calgary, 2500 University Drive North West, Calgary, Alberta T2N 1N4, Canada*

[d] *National Research Council of Canada, Ottawa, Ontario K1A 0R6, Canada*

Corresponding author: Nasser Moazzen-Ahmadi <nmoazzen@ucalgary.ca>

Keywords: CRDS, van der Waals complex, overtone, Coriolis interactions

Abstract

We report observation of the weakly-bound Ar-D_2O complex in the 3OD overtone stretch region (≈7900 cm^{-1}). The measurement was made using the FANTASIO cavity ring-down spectrometer (CRDS) combined with a 8 cm long pulsed slit nozzle valve. Several sub-bands are assigned. At 7892 cm^{-1}, the $\Sigma(0_{00})$, (201) ← $\Sigma(1_{01})$, (000) band (*para* nuclear spin species) experiences a moderate (≈0.04 cm^{-1}) perturbation between $J' = 6$ and 7. At 7903 cm^{-1}, the $\Sigma(1_{01})$, (201) ← $\Sigma(0_{00})$, (000) band (*ortho nuclear spin* species) exhibits a more complicated perturbation at about the same *J*-values. Most of the observed transitions (187) can be rotationally assigned. Finally, in the range 7913 – 7916 cm^{-1}, the $\Pi(1_{01})$, (201) ← $\Sigma(0_{00})$, (000) and $\Pi(1_{10})$, (201) ← $\Sigma(0_{00})$, (000) bands (*ortho nuclear spin species*) are observed, and their rotational analysis remains tentative.

Keywords:

Overtone spectroscopy, van der Waals complexes, Water-Argon, Supersonic expansion, Cavity ring-down spectroscopy

1. Introduction

The Ar-H_2O complex is one of the simplest weakly-bound dimers containing the water molecule. This complex has been predicted to play a role in the radiative budget of the Earth's atmosphere, along with $(H_2O)_2$, H_2O-N_2, H_2O-O_2, and H_2O-CO_2 [1]. Among these complexes, the water dimer [2–8] has attracted significant attention, leading more recently to its detection in the millimeter range at ambient temperature [9] following an earlier theoretical prediction [10]. Subsequent studies reported spectral signatures in the sub-THz [11] and explored its presence in the near-infrared regions. Another much less strongly bound complex, $(H_2)_2$, was recently detected at ambient temperature, in the first overtone region [12]. This detection highlighted the presence of bound-bound transitions at ambient temperature and at frequencies corresponding to energies significantly higher than the dissociation threshold of the complex. These studies reinforce the relevance of overtone spectroscopy for the atmospheric detection of van der Waals complexes, in addition to their importance for helping to benchmark advances in quantum chemistry.

High-resolution spectroscopic studies of the Ar-water complex provide quantitative information for the understanding of the nature and strength of the intermolecular bond linking both species, helping to test theoretical characterizations of such weakly bound complexes. This is especially true for overtone studies for which the density of states increases and the basis set size needs to be significantly increased. The underlying approximations used to make the calculations converge render the theoretical predictions harder to perform, and the validity of such approaches must be properly evaluated [13]. Theory keeps rapidly improving, but high-resolution overtone spectroscopy is still a necessary source of information to challenge and verify theoretical calculations.

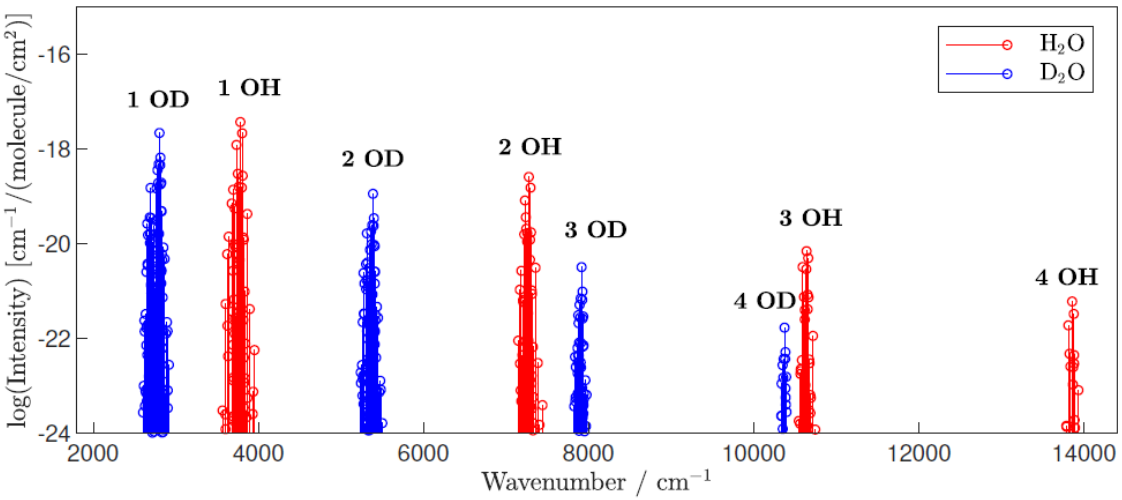

Fig. 1. Intensity of the fundamental and three first OH and OD stretch overtone bands of H_2O (in red) and D_2O (in blue) at 15 K on a log scale, taken from HITRAN. In the present paper, we study the 3OD region of Ar-D_2O.

Several challenges are faced when studying van der Waals complexes in the overtone regions. First, the absorption cross-section of overtone bands decreases greatly [14] as shown in Fig. 1. This figure presents the intensity of the stretch vibrational bands of H_2O (in red) and D_2O (in blue) monomers at 15 K on a logarithmic scale, with data taken from HITRAN [15]. The vibrational bands depicted in Fig. 1 are vibrational transitions from the ground vibrational state to $(\nu_1\nu_2\nu_3)$ = (100), (001), (200), (101), (300), (201), (400), and (301), where ν_1 (symmetric stretch), ν_2 (bend), and ν_3 (asymmetric stretch) are the vibrational quantum numbers of water. The intensity decreases by about a factor 10 or more between each successive stretch band, resulting in an intensity loss of about a factor 500 between the 1OH/OD and the 3OH/OD bands. Secondly, molecular complexes are usually produced in the laboratory using supersonic expansions in which densities are relatively low and hence absorption signals are intrinsically weak [16]. Finally, the density of molecular states increases with the frequency of excitation. This can lead to a larger number of perturbations, making the spectral signatures more difficult to analyze. Due to these factors, there is a need for highly sensitive instrumental techniques when targeting overtone spectroscopy of molecular complexes, and traditional Hamiltonians might fail to reproduce spectral signatures with experimental accuracy.

Despite these challenges, Ar-water complexes have been studied in several overtone regions. The 2OH stretch region of H_2O in Ar-H_2O was first studied at relatively low resolution by Nizkorodov et al. [17], and later studied with high-resolution spectroscopy by Vanfleteren et al. [18,19] with an earlier version of the FANTASIO spectrometer used here. The same spectrometer has also been used to probe Ar-D_2O and Ar-HDO in the (111) and (101) vibrational states of D_2O and HDO, respectively [20]. Recently, the authors of the present study and other collaborators reported new data about Ar-H_2O in the 2OH stretch region [21]. Finally, Nesbitt and co-workers [22–24] investigated the 3OH stretch region in Ar-H_2O and Ar-HOD using vibrationally mediated spectroscopy, coupling 3 lasers and recording laser-induced fluorescence to record spectra at around 116 times the calculated dissociation energy of the complex [25]. Other experimental works on the Ar-water complex include microwave [26,27] far infrared [28,29] and mid infrared [30–33] studies.

Here we present the first study of Ar-D_2O in the 3OD stretch region, observed using cavity ring-down spectroscopy (CRDS) with a signal-to-noise ratio (SNR) of up to 200 for the strongest lines. In the 7900 cm^{-1} region, studied here, the spectrum of D_2O monomer is dominated by the (201) ← (000) band, whose origin is 7899.825 cm^{-1}. Other D_2O vibrational states close to (201) are (300) at 7852.929, (022) at 7826.4, and (102) at 8054.074 cm^{-1}, but transitions to them from the ground state are weaker (especially for the latter two). Therefore, it is no surprise that the Ar-D_2O bands studied here correspond to D_2O (201) ← (000) vibrational transitions. But these Ar-D_2O bands also encounter a number of perturbations which must involve vibrational states other than (201), highlighting the challenges mentioned above.

2. Cavity ring-down apparatus

The CRDS of the FANTASIO set-up (for ‘Fourier trANsform Tunable diode and quadrupole mAss spectrometers interfaced to a Supersonic expansIOn’) [21,34,35] was used to investigate an expansion of D_2O (D214 from Eurisotop) seeded in Ar (purity 5.0 from Air Liquide). The main new technical development allowing us to record the spectra in the 3OD stretch region is the addition of a new 8 cm long pulsed slit nozzle valve in the set-up, increasing the path length in the expansion and the SNR by nearly a factor of three. The gas injection procedure was also modified, replacing the previous bubbler with a controlled evaporator mixer based on flow

controllers (F-201 and M12 from Bronkhorst). The flows used to produce Ar-D_2O in the jet were 3 standard L/min of Ar gas and 0.5 g/h of liquid D_2O. The pulsed slit valve was operated at 4 Hz with 20 ms gas pulses. The ON/OFF sorting of the ring-downs was performed in time ranges comprised between 5−20/72−248 ms after the TTL rise. The backing pressure was between 0.9 and 1 bar and the residual pressure in the chamber was about 10^{-2} mbar. The 75 cm long cavity was composed of two mirrors (109372 from Layertech) with 1000 mm radius of curvature and approximately 99.995 % reflectivity. The empty cavity ring-down time was around 77 µs. Some 200 ring-downs were averaged per spectral point, in less than 1.5 s, with between 10 to 20 of them probing the supersonic expansion. This yielded a cavity noise level of $\alpha_{min} = 1 \times 10^{-10}$ cm^{-1}. Since the molecular beam length is only about 1/10 of the cavity length, the noise equivalent absorption for the jet is $\alpha = 1 \times 10^{-9}$ cm^{-1} [34]. Wavenumber calibration was performed using a new ultra-low expansion Fabry-Perot etalon, placed under vacuum (continuous pumping during measurements giving a residual pressure of around 2×10^{-5} mbar in the etalon chamber) and temperature stabilized at 32° C [21]. Absolute wavenumber accuracy is estimated to be better than 1×10^{-3} cm^{-1} using D_2O monomer transition frequencies retrieved from HITRAN [15]. Two DFB lasers (‘Eblana Photonics’, centered at 1264 and 1268 nm; 10 mW, 1 MHz linewidth) coupled to a booster optical amplifier (BOA1250S from ‘Thorlabs’) were used to record the spectral range of interest, comprised between 7870 and 7920 cm^{-1}. The effective rotational temperature in the jet was found to be about 13 K from the relative intensities of the rotational lines in the observed spectra.

3. Observed spectra and rotational analysis

Water molecules are relatively free to rotate within an Ar-water complex, and most previous studies have thus described Ar-water in terms of a pseudo-diatomic molecule whose different “vibrational” states each correlates with a particular water monomer rotational state. Here we follow this scheme and label sub-states of Ar-D_2O with the notation $|M_j|(j_{kakc})$. The j_{kakc} label refers to the rotational level of D_2O, using conventional asymmetric top notation. M_j is the projection of the rotational angular momentum (j) of the D_2O on the intermolecular axis of the complex. The $|M_j| = 0, 1, 2, ...$ values are labeled as Σ, Π, Δ, ..., respectively, and the total rotational angular momentum of the complex is defined using the J quantum number.

The *ortho*/*para* nuclear spin classification of the water molecule is preserved inside the complex. In the ground vibrational state, D_2O rotational levels with (k_a, k_c) = (even, even) or (odd, odd) correspond to the *ortho* (spin weight = 6), while those with (even, odd) or (odd, even) correspond to *para* (spin weight = 3) spin species. In the (201) excited vibration, these labels are reversed. Since no spin relaxation is expected to occur in the supersonic expansion, the most highly populated initial states of Ar-D_2O in our experiment are the lowest lying levels of each species, $\Sigma(0_{00})$ for *ortho* and $\Sigma(1_{01})$ for *para* (we know from previous work that $\Pi(1_{01})$ lies about 11 cm^{-1} higher in energy [29]).

Assignment, simulation, and fitting of the spectra were done using the linear molecule option of the PGOPHER software package [36]. Diagonal rotational energies are given by:

$$\langle \Sigma_1 | H | \Sigma_1 \rangle = B \times J(J+1) - D \times [J(J+1)]^2 + H \times [J(J+1)]^3$$

$$\langle \Pi_1 | H | \Pi_1 \rangle = B \times [J(J+1) - 1] - D \times [J(J+1) - 1]^2 + H \times [J(J+1) - 1]^3$$

Perturbations in the spectrum involve homogeneous (Fermi-type) parameters, W, which connect Σ to Σ, or Π to Π, states, along with parameters W_B and W_D to allow for centrifugal distortion of the Fermi interaction. The Coriolis parameters, G, which connect Σ to Π states. These off-diagonal interaction matrix elements are given by:

$$\langle \Sigma_1 | H | \Sigma_2 \rangle = W(\Sigma_1,\Sigma_2) + W_B(\Sigma_1,\Sigma_2) \times J(J+1) + W_D(\Sigma_1,\Sigma_2) \times [J(J+1)]^2,$$

$$\langle \Pi_1 | H | \Pi_2 \rangle = W(\Pi_1,\Pi_2),$$

$$\langle \Sigma_1 | H | \Pi_2 \rangle = G(\Sigma_1,\Pi_2) \times [2J(J+1)]^{1/2}.$$

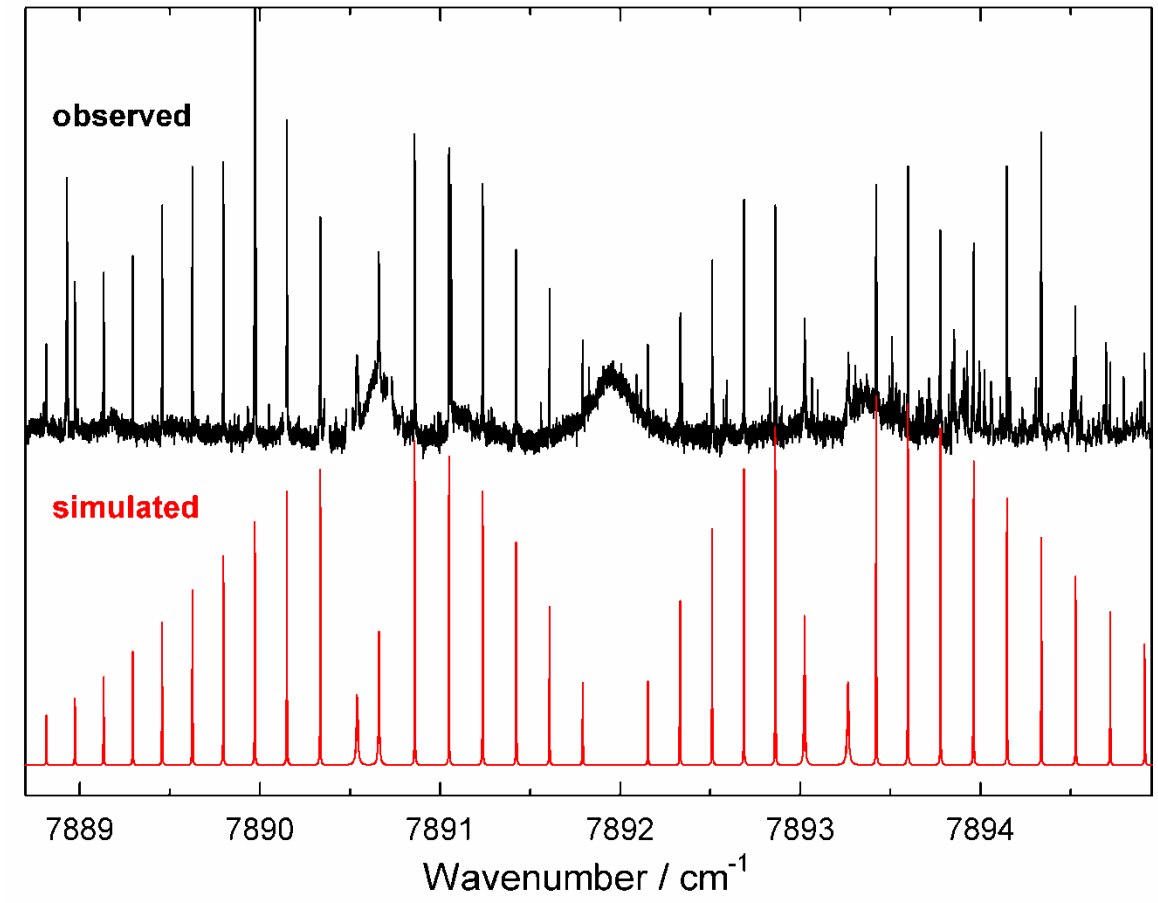

Fig. 2. Observed and simulated spectra of the $\Sigma(0_{00})$, (201) $\leftarrow\Sigma(1_{01})$, (000) band of Ar-D_2O. A perturbation around $J'= 7$ causes the dip in line intensity around 7890.5 and 7893.3 cm^{-1} (see text). The broad absorption features are probably associated to D_2O dimer.

3.1. The $\Sigma(0_{00})$, (201) $\leftarrow\Sigma(1_{01})$, (000) band, 7892 cm^{-1}

Figure 2 shows the first of the observed Ar-D_2O bands. This is a straightforward $\Sigma \leftarrow \Sigma$ transition and we know that it must involve the *para* species because the lower state rotational parameters agree with those known for the ground $\Sigma(1_{01})$ state. Vibrational assignment as the $\Sigma(0_{00}$-), (201) $\leftarrow\Sigma(1_{01})$, (000) band is described below in Sec. 4. Observed line positions and rotational assignments are listed in Table S-1 of the Supplementary Information. There is a large perturbation in the upper state between $J'= 6$ and 7 as demonstrated by the residuals of the fit shown with black dots in Fig. 3. Upper state levels with $J' \leq 6$ are 'pushed down' by the perturbation, while those

with $J' \geq 7$ are 'pushed up', making it evident that the perturbing state comes from above and has a smaller rotational constant. We tried simulating the perturber as a Σ state (with a homogeneous interaction parameter, W), or as a Π state (with Coriolis interaction parameter, G), and the latter choice was significantly better. The red dots in Fig. 3 show the residuals from the Π-perturber fit, whose root mean square deviation (rmsd) is 0.00036 cm^{-1}. The resulting parameters are given in Table 1.

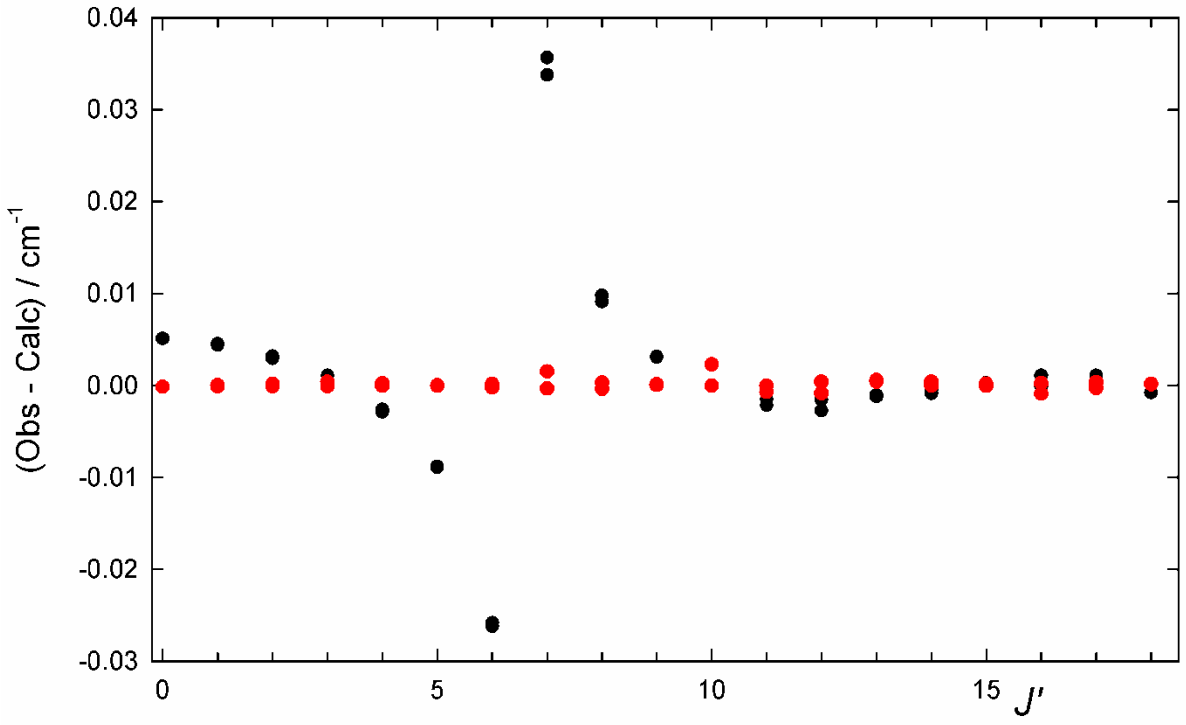

Fig. 3. Residuals from fits to the $\Sigma(0_{00})$, (201) ←$\Sigma(1_{01})$, (000) band. For the red dots, the perturbation is included in the calculation, but not for the black ones. The double dots for most J-values arise from P- and R-branch lines.

Table 1. Molecular parameters for the $\Sigma(0_{00})$, (201) ← $\Sigma(1_{01})$, (000) band of Ar-D_2O (in cm^{-1}). [a]

	$\Sigma(0_{00})$, (201)	Π (7893)
ν_0	7891.9733(2)	7893.071(3)
B'	0.0904307(66)	0.068841(41)
D'	$-2.930(49) \times 10^{-6}$	
H'	$-7.014(98) \times 10^{-9}$	
$G[\Sigma(0_{00}), \Pi(7893)]$	0.007483(37)	
n	36	
rmsd	0.00036	
	$\Sigma(1_{01})$, (000)	
B'' [b]	0.09103344	
D'' [b]	1.76655×10^{-6}	
H'' [b]	-4.5×10^{-10}	

[a] Quantities in parentheses are 1σ from the least-squares fit, in units of the last quoted digit. *n* is the number of observed lines and rmsd is the root mean square average error in the fit.

[b] Ground state parameters for the $\Sigma(1_{01})$ lower state are from [21].

Close examination of the spectrum shows that the $\Sigma(0_{00})$, (201) ←$\Sigma(1_{01})$, (000) band transitions which are the most perturbed (J' = 6 and 7) demonstrates significant lower intensity and extra broadening. It is therefore likely that the perturber state is affected by predissociation, sharing the resulting consequences with the perturbed $\Sigma(0_{00})$, (201) state. Fortunately, the model previously defined enables us to simulate this effect, as shown in Fig. 2. By ascribing a Lorentzian width of 0.04 cm^{-1} to the Π (7893) state, it is possible to match the observed spectrum satisfactorily. Because of this predissociation effect, expected lines from the perturber are likely to be too wide to be observed.

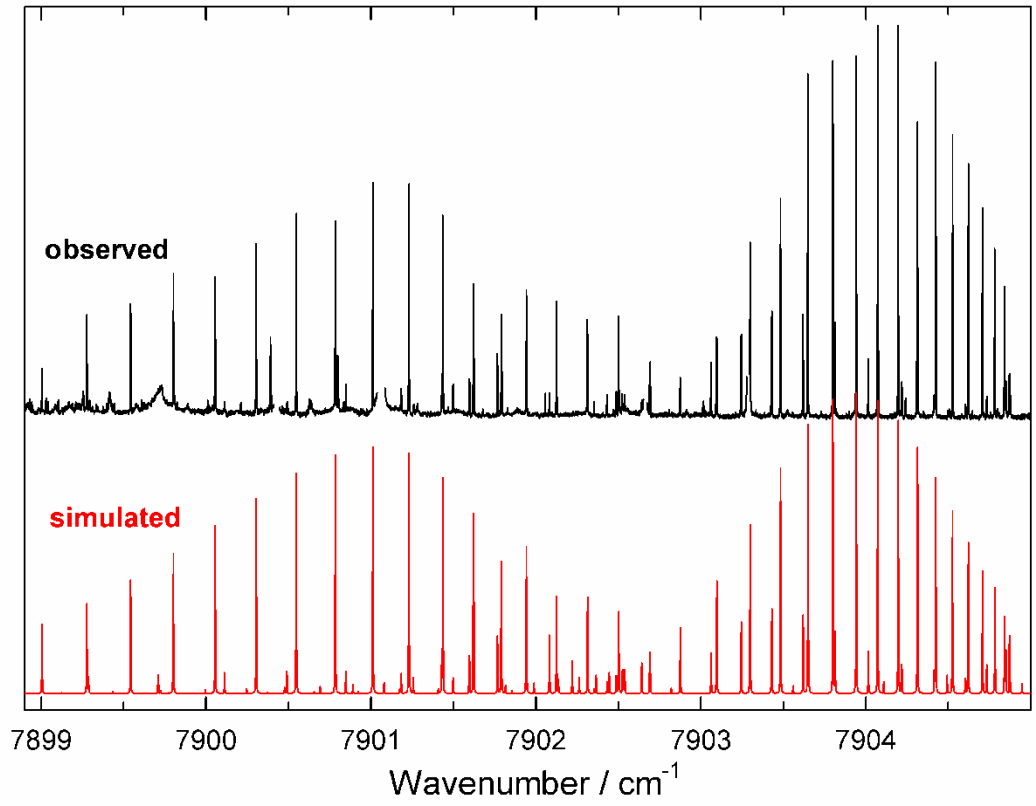

Fig. 4. Observed and simulated spectra of the $\Sigma(1_{01})$, (201) ← $\Sigma(0_{00})$, (000) band of Ar-D_2O.

3.2. The $\Sigma(1_{01})$, (201) ← $\Sigma(0_{00})$, (000) band, 7903 cm^{-1}

Figure 4 shows the 7903 cm^{-1} range, with two overlapping $\Sigma \leftarrow \Sigma$ transitions involved among which the strongest band reported in this work. From the lower state parameters, these 7899 to 7905 cm^{-1} range bands originate from the ground state of the *ortho* species, $\Sigma(0_{00})$, (000). The dominant band here corresponds to $\Sigma(1_{01})$, (201) ← $\Sigma(0_{00})$, (000), the inverse of the 7892 cm^{-1} band. The weaker band could possibly be assigned as $\Sigma(2_{11})$, (300) ← $\Sigma(0_{00})$, (000) (see Sec. 4). Rotational assignment of the two bands, confusing at first, could be achieved with the help of ground state combination differences. These assignments are listed in Table S-2. There is evidence for interaction between the two upper states and, after some trial and error, we eventually found a

scheme which fitted the spectrum very well and which also explained a number of additional weak lines in the observed spectrum.

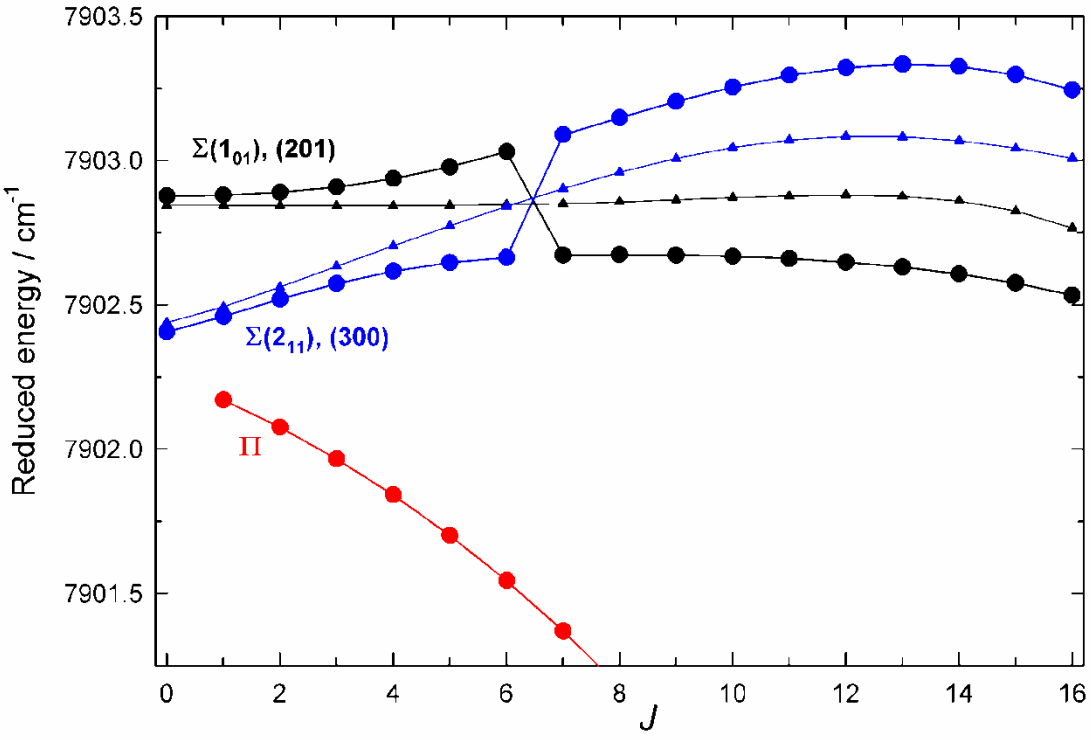

Fig. 5. Upper energy level diagram related to the bands observed around 7903 cm^{-1} band in Ar-D_2O. For clarity, rotational energies are reduced by the quantity $B_{eff} \times J(J + 1)$, with $B_{eff} = 0.090$ cm^{-1}. The scheme includes a Fermi-type interaction between the two upper Σ states. In addition, a Coriolis coupling is included between the $\Sigma(2_{11})$, (300) state (blue) and a dark Π state (red). The Σ states are highly mixed for all J-values, and their color-coded labels (from PGOPHER) may be misleading: it may be helpful to think of the upper Σ state continuing to be black above $J = 6$, and the lower Σ state continuing to be blue. Dots illustrate the actual (fully perturbed) situation while triangles illustrate what happens if the Fermi interaction is turned off and the Coriolis interaction remains included.

This scheme is illustrated in Fig. 5 which presents a reduced energy level diagram for the excited states. Two Σ states are coupled by a homogeneous (Fermi-type) interaction, and the lower Σ state is also perturbed by a Coriolis-type interaction with a Π state located just below it. The Π

state has a smaller *B*-value, so it moves away to lower energy as *J* increases while at the same time, the magnitude of the Coriolis coupling increases. The lower Σ state is thus 'pushed' up so that it would cross over the other Σ state between $J = 6$ and 7, leading to an avoided crossing. As we adjusted this 3-states scheme to fit the observed spectrum, we were pleased to find that it predicted some perturbation-allowed transitions to the Π state that could explain weak lines in the spectrum. These assignments were furthermore supported by ground state combination differences. Adding these weak transitions to the fit firmly anchored the position of the Π state. Table 2 lists the final set of parameters for this band, in which 66 transitions were fit with a rmsd of 0.00050 cm^{-1}.

Table 2. Molecular parameters for the bands observed in the 7903 cm^{-1} region of Ar-D_2O (in cm^{-1}).[a]

	$\Sigma(1_{01})$, (201)	$\Sigma(2_{11})$, (300)	Π (7902)
ν_0	7902.8446(8)	7902.4388(10)	7902.3202(9)
B'	0.089829(53)	0.09454(12)	0.079541(54)
D'	$-6.62(68) \times 10^{-6}$	$23.2(12) \times 10^{-6}$	
H'	$-2.59(12) \times 10^{-8}$	$2.91(38) \times 10^{-8}$	
W [$\Sigma(1_{01})$, $\Sigma(2_{11})$]	0.1181(15)		
W_B [$\Sigma(1_{01})$, $\Sigma(2_{11})$]	$2.272(44) \times 10^{-3}$		
W_D [$\Sigma(1_{01})$, $\Sigma(2_{11})$]	$-5.14(29) \times 10^{-6}$		
G [$\Sigma(2_{11})$, Π (7902)]	0.05566(20)		
n	66		
rmsd	0.00050		
	$\Sigma(0_{00})$, (000)		
B''[b]	0.093262186		
D''[b]	2.60637×10^{-6}		
H''[b]	-8.026×10^{-11}		

[a] Quantities in parentheses are 1σ from the least-squares fit, in units of the last quoted digit. *n* is the number of observed lines and rmsd is the root mean square average error in the fit.

[b] Ground state parameters for the $\Sigma(0_{00})$ lower state are from [21].

We found that the relative intensities of the various lines in the 7903 cm^{-1} band could be best reproduced by giving relative transition dipole moments of -0.4 and 0.0 to the $\Sigma(2_{11})$ and Π components, respectively, relative to $\Sigma(1_{01})$. Parts of the band matched better by including some Π intensity, but not consistently. The weak transitions involving the Π (7902) state thus borrow most or all of their strength from mixing with the two other states. The main failure of the simulation is that lines of the $\Sigma(2_{11})$ band with $J' > 9$ (and of the Π (7902) band with $J' > 6$) are predicted with significant intensity although they are absent in the observed spectrum. This probably demonstrates the onset of predissociative broadening in both states, possibly due to the Π (7902) state itself, or to interaction with an unknown fourth state.

Earlier we stated that the interaction between the $\Sigma(1_{01})$, (201) and $\Sigma(2_{11})$, (300) states was homogeneous (that is, not *J*-dependent), but this is not entirely true. In fact, the parameters W_B and W_D in Table 2 contain significant *J*-dependence, and they are essential for the good fit. These parameters could be thought of as a simple rotational dependence of the basic homogeneous perturbation, but more likely they express a second order Coriolis effect. For example, one of the Σ states could be Coriolis coupled to a nearby Π state (with *J* dependence) and the Π state coupled back to the other Σ state (more *J* dependence). Of course, we already have a nearby Π state coupled to $\Sigma(2_{11})$! It turns out that if W_B and W_D are constrained to zero, a moderately good fit can be regained by introducing a Coriolis interaction between the $\Sigma(1_{01})$ and Π states. But the fit with W_B and W_D and no $\Sigma(1_{01})$ - Π Coriolis is still much better in terms of rmsd and simulated intensities than the fit with $\Sigma(1_{01})$ - Π Coriolis and no W_B and W_D. This could be further evidence of unknown interactions with additional states beyond the three in our model.

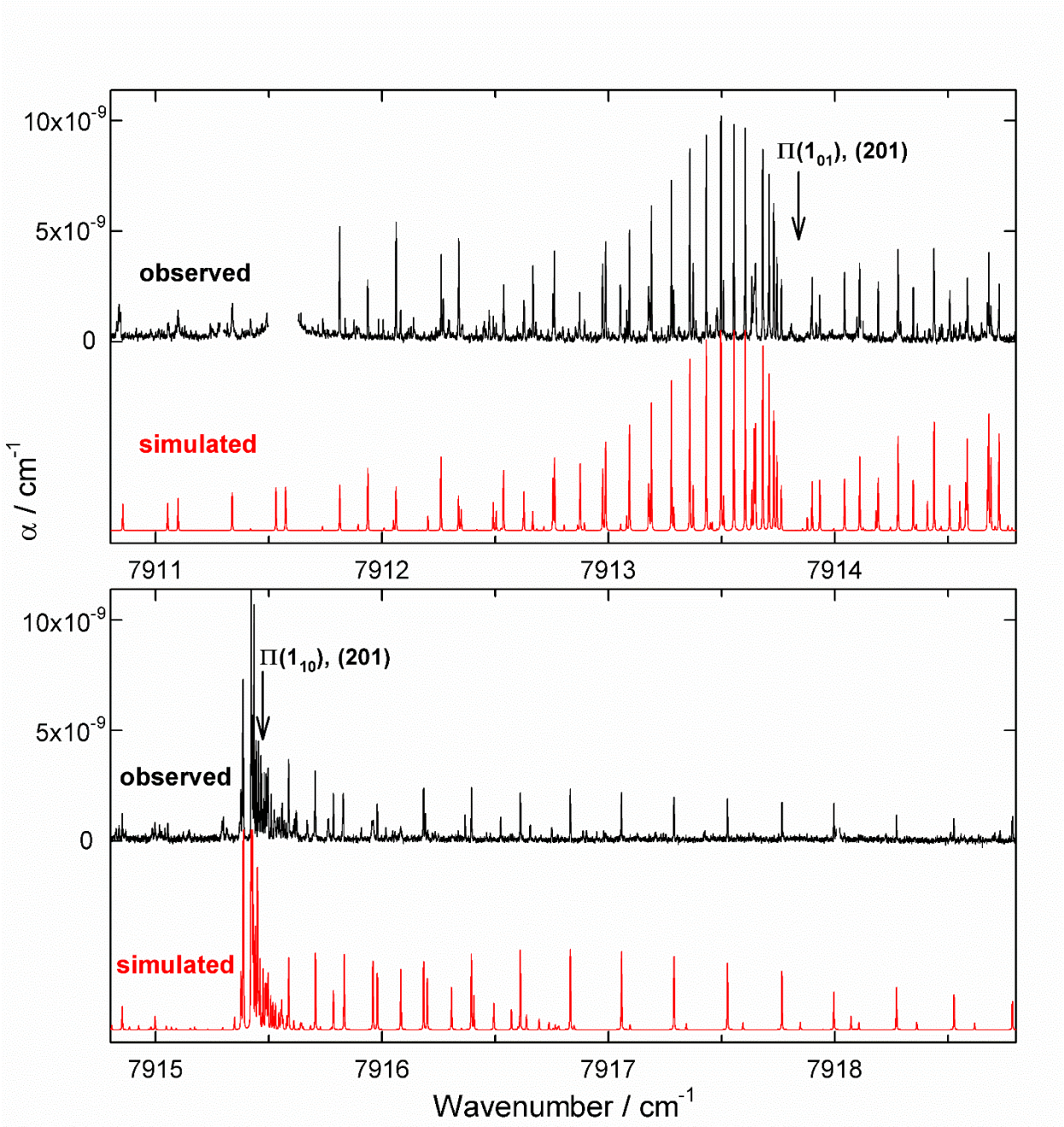

Fig. 6. Observed and simulated spectra of the $\Pi(1_{01})$, (201) $\leftarrow\Sigma(0_{00})$, (000) (upper panel) and $\Pi(1_{10})$, (201) $\leftarrow\Sigma(0_{00})$, (000) (lower panel) bands of Ar-D_2O. The band origins are marked with arrows.

3.3. The $\Pi(1_{01})$, (201) ← $\Sigma(0_{00})$, (000) and $\Pi(1_{10})$, (201) ← $\Sigma(0_{00})$, (000) bands, 7912 – 7918 cm^{-1}

Two $\Pi \leftarrow \Sigma$ transitions with expected *Q*-, *P*-, and *R*-branches are observed in the 7912-7918 cm^{-1} range. They are presented in Fig. 6. They again originate in the ground *ortho* state, $\Sigma(0_{00})$, (000), and from their positions can be assigned to the upper states $\Pi(1_{01})$, (201) and $\Pi(1_{10})$, (201) as indicated in Fig. 6. Since they originate from an *e*parity sigma state, their *Q*-branch involve upper state levels with *f* parity [37], and *P*- and *R*-branches involve levels with *e* parity.

The most easily assigned part of the spectrum is the prominent $\Pi(1_{01})$, (201) *Q*-branch in the 7912 – 7914 cm^{-1} region, which can be followed from $J = 1$ to 19, while showing a relatively small perturbation at $J = 5$. The $\Pi(1_{01})$, (201) *P*- and *R*-branches suffer a large perturbation between $J' = 7$ and 8, which is responsible for the gap in the spectrum between 7914.8 and 7915.3 cm^{-1}. The help of ground state combination differences was required to number lines up to $J' = 13$. Lines then broaden and disappear, presumably due to interactions with a short-lived perturber.

The $\Pi(1_{10})$, (201) *P*- and *R*-branches could be assigned up to $J' = 17$, experiencing a moderate perturbation at very low *J*-values and a small one around $J' = 12$. Details of the rotational assignments and observed line positions are given in Table S-3 of the Supplementary Information. The $\Pi(1_{10})$, (201) *Q*-branch (around 7919.5 cm^{-1}) is strongly perturbed and the lines could not be reliably numbered. In this case, there are no combination differences available to establish definite rotational assignments, and the best we can do is to propose an approximate scheme, described below, to qualitatively simulate the observed spectrum.

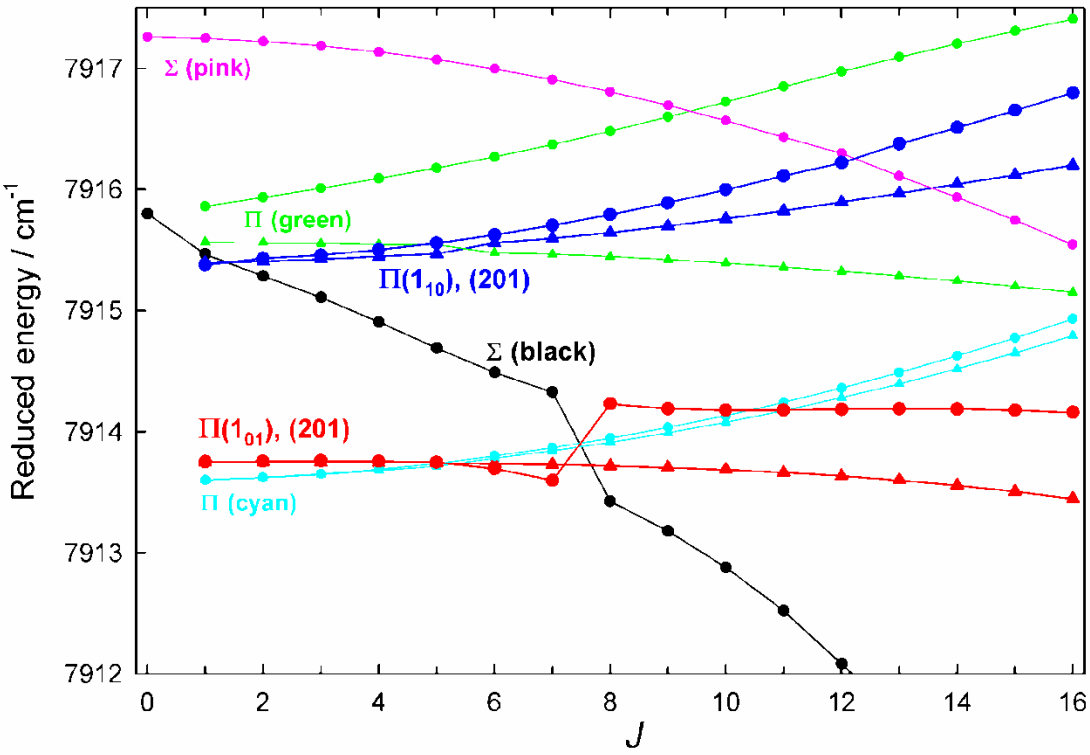

Fig. 7. Energy level diagram simulating the 7914 and 7915 cm^{-1} bands of Ar-D_2O. For clarity, rotational energies are reduced by the quantity $B_{\text{eff}}J(J+1)$, with $B_{\text{eff}} = 0.090$ cm^{-1}. Dots and triangles indicate levels with parity *e* and *f*, respectively. The main states carrying all the transition strength are $\Pi(1_{01})$, (201) in red, and $\Pi(1_{10})$, (201) in blue. A Σ (black) dark state crosses $\Pi(1_{10})$ between $J = 1$ and 2, and $\Pi(1_{01})$ between $J = 7$ and 8, causing perturbations to their *e* components. The Π (green) state has widely split *e* and *f* components. The *e* component interacts significantly with Σ (black) state and the *f* component qualitatively explains a perturbation around $J = 5$ in the *f* levels of $\Pi(1_{10})$. The Σ (pink) and Π (cyan) dark states are required to explain other small observed perturbations. As emphasized in the text, this interaction scheme is tentative.

We have worked out a possible, but not definite, interaction scheme. It is presented in Fig. 7, to account for the many observed perturbations, involving four dark states and eight interaction matrix elements. It reproduces reasonably well the band shapes and the observed line positions, as illustrated in Fig. 6. The point of our analysis is to show that an approximate solution is possible and that it requires a number of perturbing states. A dark state called Σ (black) crosses the $\Pi(1_{01})$, (201) state from above between $J = 7$ and 8, explaining the large perturbation noted in its *P*- and *R*-branches. It is assumed to be a Σ state because any other state (Π, Δ,...) would involve a *f* parity

component and cause large perturbation in the *Q*-branch, that are unobserved. The small *Q*-branch perturbation at $J = 5$ is explained by the *f* component of a Π (cyan) dark state, coming from below. The Σ (black) state also helps to explain a perturbation observed in the *e* component of the $\Pi(1_{10})$ state around $J = 1$ to 3, and the Π (cyan) state similarly causes small perturbations in the *e* component of $\Pi(1_{01})$ at $J = 5$ and 10, as observed.

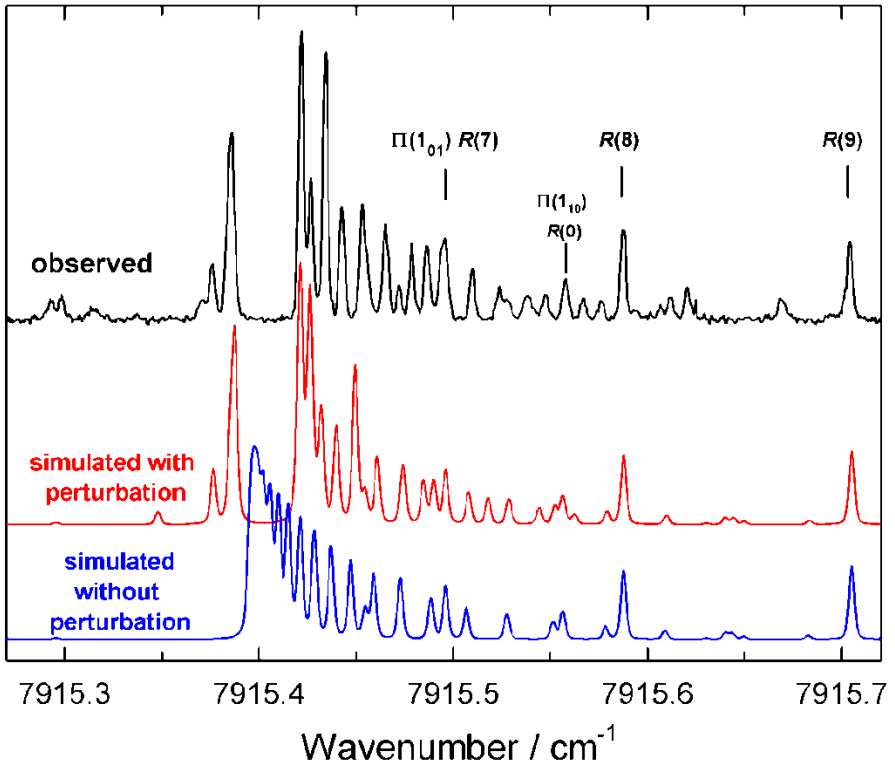

Fig. 8. Expanded view of the *Q*-branch region of the $\Pi(1_{10})$, (201) ←$\Sigma(0_{00})$, (000) band of Ar-D_2O, with the experimental spectrum in the upper trace. The red simulation (middle trace) is the same as shown in Fig. 6 and explained in Fig. 7. For the blue simulation (lower trace), the interaction between the *f* components of $\Pi(1_{10})$ and Π (green), shown in Fig. 7, is turned off.

As noted above, it is not possible to confidently assign rotational quantum numbers in the perturbed $\Pi(1_{10})$, (201) band *Q*-branch at 7915.4 cm^{-1}. However, a qualitative simulation can be made by introducing the state labeled Π (green) in Fig. 7 so that its *f* component crosses the *f* component of $\Pi(1_{10})$ from above around $J = 5$. This level crossing splits the $\Pi(1_{10})$ *Q*-branch,

inducing a gap between 7915.39 and 7915.42 cm^{-1} which is illustrated in Fig. 8. Similar observations were reported in the literature (see Figs. 3 and 4 of [38]). Note that the *Q*-branch lines were neither assigned nor fitted. Nevertheless, the overall agreement looks reasonable. We were also pleasantly surprised to find that including the related Π (green) *e* levels and a Coriolis interaction to the Σ (black) state enabled the least-squares fit to be improved by a factor of two.

The final fit gives a satisfactory rmsd of 0.00049 cm^{-1}. It includes 85 lines: 25 for the $\Pi(1_{01})$ *e* upper state (J' = 1 to 13); 17 for $\Pi(1_{01})$ *f* (J' = 1 to 17); 32 for $\Pi(1_{10})$ *e* (J' = 1 to 17); 8 for Σ (black) (J' = 5 to 9); and 3 for Π (cyan) (J' = 5). The best simulation (Fig. 6) has relative transition moments of 1.0 for the $\Pi(1_{01})$, (201) band, 0.8 for the $\Pi(1_{10})$, (201) band, and 0 for the other (perturbing) bands. The weak transitions involving the Σ (black) state borrow their strength from mixing with the two bright states. The 35 parameters of the fit are listed in Table 3. Note the six parameters (footnote b) which were manually adjusted to qualitatively simulate the 7915.4 cm^{-1} *Q*-branch as described in the preceding paragraph (for the Π*f*(1_{10}), (201) and Π*f* (green) states, and their interactions). Note also the three parameters (footnote d) which were adjusted manually to avoid instability in the fit. Each of these three could be varied by roughly 10% without greatly changing the fit, but each was still needed to maintain the good fit. We emphasize here that, even though the fit (Table 3) and simulation (Figs. 6 – 8) are good, they are not intended to be a unique solution for this observed spectrum, but rather serve to illustrate that a reasonably good fit is possible, and that it seems to require at least four perturbing states in addition to the main upper states, $\Pi(1_{01})$, (201) and $\Pi(1_{10})$, (201). It is the rotational assignments in Table S-3 which are more meaningful, and not so much the many parameters in Table 3.

Table 3. Parameters for the Π(1_{01}), (201) and Π(1_{10}), (201) states of Ar-D_2O (in cm^{-1}). [a]

	Π*e*(1_{01}), (201)	Π*f*(1_{01}), (201)	Π*e*(1_{10}), (201)	Π*f*(1_{10}), (201)	Σ(black)
ν_0	7913.8432(2)	7913.8404(4)	7915.4723(5)	7915.488 [b]	7915.855(87)
B′	0.092391(28)	0.089814(13)	0.095775(18)	0.0935 [b]	0.0647(14)
D′	4.92(30)× 10^{-6}	3.84(11)× 10^{-6}	1.13(13)× 10^{-6}	2 × 10^{-6} [b]	-1.06(12)× 10^{-4}
H′		1.48(25) × 10^{-9}	-3.67(26) × 10^{-9}		-3.73(56) × 10^{-7}

	Π (cyan)	Σ(pink)	Π*e* (green)	Π*f* (green)
ν_0	7913.6869(8)	7917.260(5)	7915.653 [d]	7915.653 [b]
B′	0.094696(23) [c]	0.0837 [d]	0.09478 [d]	0.0885 [b]

W [Π*e* (1_{01}), Π (cyan)]	0.01046(37)
W [Π*f* (1_{01}), Π (cyan)]	0.00317(46)
G [Π*e* (1_{01}), Σ (black)]	0.03833(103)
G [Π*e* (1_{10}), Σ (black)]	0.0263(21)
G [Π*e* (1_{10}), Σ (pink)]	0.001959(77)
G [Σ (black), Π*e* (green)]	0.0956(102)
G [Σ (black), Π (cyan)]	-0.002 [d]
W [Π*f* (1_{10}), Π*f* (green)]	0.035 [b]
n	85
rmsd	0.00049

[a] Quantities in parentheses are 1σ from the least-squares fit, in units of the last quoted digit. *n* is the number of observed lines and rmsd is the root mean square average error in the fit. Ground state parameters for the Σ(0_{00}) lower state are from [28] (see Table 2).

[b] These 6 parameters for Π*f*(1_{10}), (201), Π*f* (green) and their interaction were adjusted manually to give a qualitative simulation of the Π*f*(1_{10}), (201) *Q*-branch, as shown in Fig. 8.

[c] For the Π (cyan) state, *q* = -0.000565(35) cm^{-1}, meaning that *B* = 0.094414 cm^{-1} for the *e* component, and *B* = 0.094979 cm^{-1} for the *f* component.

[d] These 3 parameters without uncertainties were adjusted manually to avoid instability in the least-squares fit.

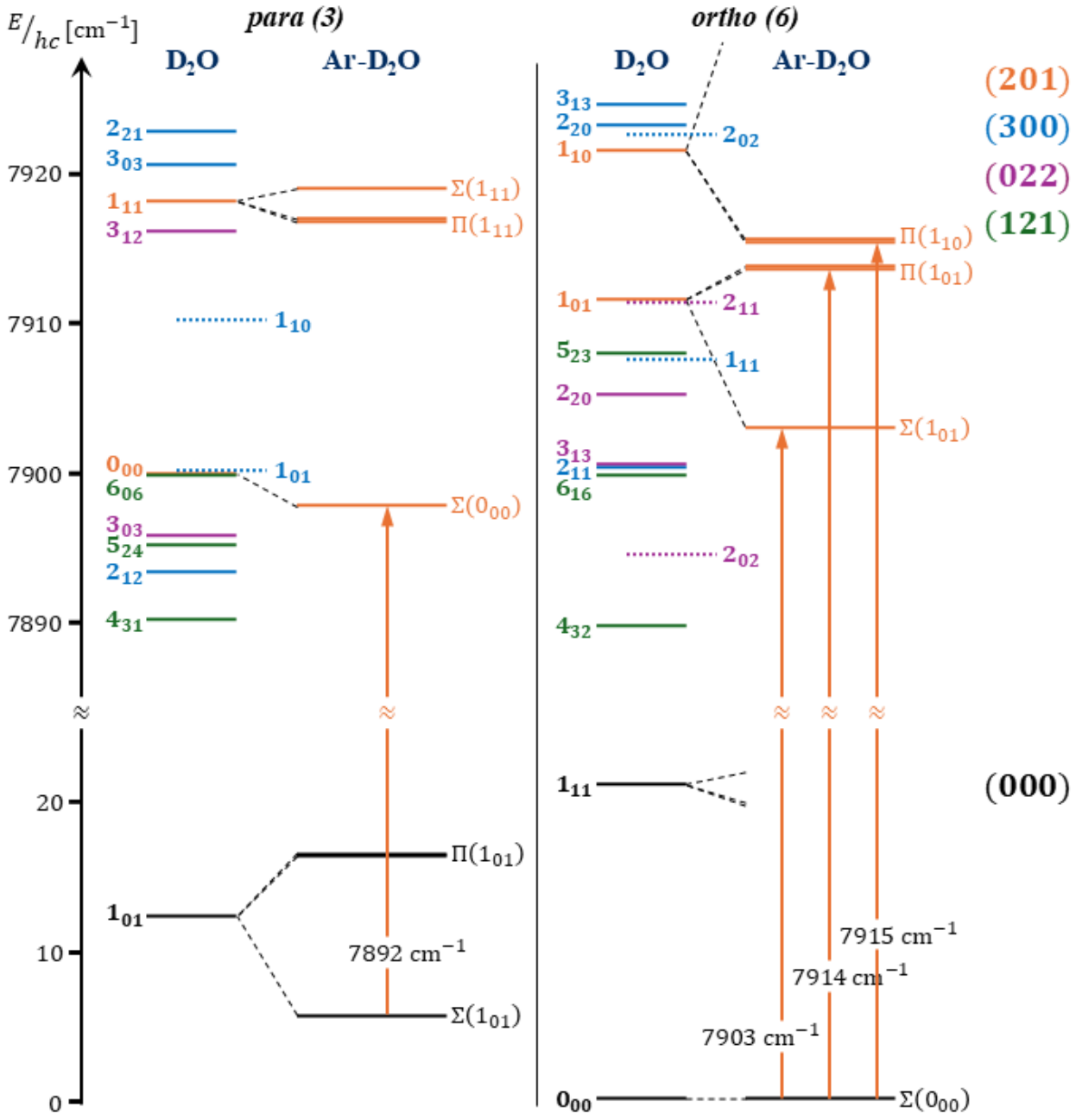

Fig. 9. Schematic D_2O energy level diagram in the ground and excited vibrational states showing the correlation with Ar-D_2O sub-states. The distinct *para* and *ortho* nuclear spin species of D_2O and Ar-D_2O are shown on the left and right panels, respectively. The nuclear spin statistical weight is indicated under bracket. Vertical arrows show the four Ar-D_2O bands studied here. D_2O levels [15,39–41] are color-coded as indicated by labels on the right-hand side. Ar-D_2O energies are taken from ground state predictions [42] and are shifted by D_0 (95.3 cm^{-1}) with respect to D_2O levels. The various D_2O (300), (022), and (121) levels can possibly give rise to Ar-D_2O states responsible for the many observed perturbations. Dotted energy levels include one quantum of van der Waals stretch, n_s = 1 (≈35 cm^{-1}) [42]

and their energy is only approximate. The (121) levels shown here lie above the Ar-D_2O dissociation threshold by at least 120 cm^{-1}, and are included on the (unlikely) chance that they still might perturb the Ar-D_2O bands.

4. Vibrational assignments

As mentioned in the introduction, the spectrum of D_2O monomer in the region studied here is dominated by the (201) ← (000) band (7899.825 cm^{-1}). Other nearby D_2O bands are significantly weaker: (300) ← (000) (7852.929 cm^{-1}); (022) ← (000) (7826.4 cm^{-1}); and (102) ← (000) (8054.074 cm^{-1}). The assignment of the four main Ar-D_2O bands is straightforward because all are located within 2 or 3 cm^{-1} of the positions predicted using known D_2O and Ar-D_2O energies. Any alternate assignments would be off by at least 50 cm^{-1}.

The tentative assignment of the dark states we have included in the various interaction schemes is discussed here below. Figure 9 shows a schematic representation of D_2O and Ar-D_2O energy levels in the ground and excited vibrational states. The *ortho*/*para* nuclear spin classification of the water molecule is preserved upon complexation, so the assignment can be done separately as shown in the two panels of Fig. 9. In addition to the D_2O levels of the (201) vibration which correlate with the four observed Ar-D_2O bands, Fig. 9 also shows other D_2O vibrational levels. Note that the dotted D_2O energy levels in the figure are approximate estimates for excited Ar-D_2O states with one quantum of the intermolecular van der Waals stretch mode. Following earlier examples [42,43], we label these stretch states, for example, as follows: n_s = 1, (1_{01}), (300).

Starting with the $\Sigma(0_{00})$, (201) band of *para* Ar-D_2O at 7892 cm^{-1}, we introduced the Π (7893) dark state. The Π state origin (7893.07 cm^{-1}) is about 1.1 cm^{-1} above that of $\Sigma(0_{00})$, (201). It has a rather small effective *B*-value (0.071 cm^{-1}) and the transitions show significant homogeneous widths (0.04 cm^{-1}). By looking at Fig. 9, Possible candidates for this perturber are: $\Pi(2_{12})$, (300); $\Pi(3_{03})$, (022); or n_s = 1, $\Pi(1_{01})$, (300) (the latter might be expected to have a small *B*-value). Alternatively, the (121) levels shown in Fig. 9 could also be suggested but those lie far above their dissociation limit and would thus have significant predissociative broadening, possibly too much for their transitions to be observed. Overall, without stronger evidence, we do not assigned the Π (7893) perturbing state.

Next, the analysis of the $\Sigma(1_{01})$, (201) band of *ortho* Ar-D_2O at 7902.8 cm^{-1} involves the Σ dark state at 7902.4 cm^{-1} and the Π (7902) state at 7902.3 cm^{-1}. The fact that the Σ perturber has significant transition strength of its own suggests that it involves the (300) vibration, because the D_2O $2\nu_2 + 2\nu_3$ band is much weaker than the $3\nu_1$ band. This Σ dark state is therefore assigned to (2_{11}), (300) as already stated in Sec. 3.2. The strength of the Coriolis interaction between the two dark states involved in the analysis (G [$\Sigma(2_{11})$, Π (7902)] = 0.05566 cm^{-1}) further suggests that they both belong to the same D_2O vibrational state. Likely assignments would then be $\Pi(2_{11})$, (300) or n_s = 1, $\Pi(1_{11})$, (300). The former would explain the large Coriolis coupling and would imply that the $\Sigma(2_{11})$ and $\Pi(2_{11})$ states lie very close together (Δ= 0.12 cm^{-1}). The latter might explain the smaller observed B value of the Π state due to the van der Waals bond stretch excitation but perhaps not the strong Coriolis parameter. The assignment of the Π (7902) state thus remains uncertain.

Finally, there are many perturbing states in the 7913 - 7916 cm^{-1} region, perhaps the most significant ones being those labelled Σ (black) and Π (green). In the immediate vicinity of 7915 cm^{-1}, Fig. 9 seems to present a shortage of dark states. The closest candidates have rather uncertain positions because they involve n_s = 1. It could also be that additional higher excited overtone stretching states are to be involved. Additionally, as there exist large shifts between some D_2O levels and their related Ar-D_2O states, true locations of Ar-D_2O states can easily be several cm^{-1} away from that suggested by the correlated D_2O rotational level. Overall, we do not have any good suggestions for the assignments of the perturbing states in this region, which is why we use colors to label them in Table 3 and Fig. 7.

5. Lifetimes and conclusions

The spectra in Figs. 2, 4, 6, and 8 are simulated using an effective rotational temperature of 13 K and a Voigt line profile with Gaussian and Lorentzian full width at half maximum (FWHM) values of 0.0026 and 0.0012 cm^{-1}, respectively. The Gaussian contribution was retrieved by estimating the rotational temperature of the complex and assuming an equivalent translational temperature. The Lorentzian contribution is determined by fitting 33 of the most intense transitions in the 7903 cm^{-1} band. The same widths worked well for the other bands, except as noted for some

broadened lines. The Ar-D_2O predissociation lifetime extracted from this Lorentzian contribution is around $\tau = 3 - 8$ ns. The large uncertainty results from the large standard deviation on the Lorentzian FWHM. This lifetime is in the same range as most other values determined for Ar-water in different vibrational states [18,19,21,33].

In conclusion, four main bands are observed for Ar-D_2O in the second OD overtone region with a SNR of up to 200 achieved using the FANTASIO CRDS experiment [21]. They are assigned to the $\Sigma(0_{00})$, (201) $\leftarrow\Sigma(1_{01})$, (000) transition of the *para* nuclear spin species, and to the $\Sigma(1_{01})$, (201) $\leftarrow \Sigma(0_{00})$, (000), $\Pi(1_{01})$, (201) $\leftarrow \Sigma(0_{00})$, (000), and $\Pi(1_{10})$, (201) $\leftarrow \Sigma(0_{00})$, (000) transitions of the *ortho* species. Various perturbations affecting line positions and intensities are observed. Those in the *para* species could be analyzed, involving one dark Π state. Tentative, and more complicated perturbation schemes were discussed for those in the *ortho* species. One, for $\Sigma(1_{01})$, (201), involves two (Σ and Π, the former assigned to (2_{11}), (300)) dark states. The other, for $\Pi(1_{01})$, (201) and $\Pi(1_{10})$, (201), possibly involves four dark states in addition to the bright ones. None of the dark states, but (2_{11}), (300) could be firmly identified.

This work was made possible as a result of a series of improvements made on the FANTASIO apparatus and brings confidence that future studies in even higher vibrational excited states, i.e. the 4OD and 4OH stretch regions, should be possible for water-containing complexes.

Acknowledgments

The ULB and SQUARES service are acknowledged for the loan of the FANTASIO set-up. This work was funded by the Action de Recherches Concertées (ARC, Grant No. ARC iBEAM-18/23-090), the FNRS CDR (Grant No. J.0113.23) and MIS (Grant No. F.4038.24). R.G. is a FRIA grantee of the Fonds de la Recherche Scientifique (FNRS) and thanks the financial support of UCLouvain and the Fédération Wallonie-Bruxelles through Fonds Spéciaux de Recherche (FSR) and ARC. N. M.-A. acknowledges the Natural Sciences and Engineering Research Council of Canada for its financial support.

MH thanks FEME for so many fruitful and friendly exchanges over the years

Author Declarations

Conflict of interest

The authors have no conflicts to disclose.

Data Availability

The authors confirm that the data supporting the findings of this study are available within the article or available upon reasonable request.

References

[1] H.G. Kjaergaard, T.W. Robinson, D.L. Howard, J.S. Daniel, J.E. Headrick, and V. Vaida, J. Phys. Chem. A **107**, 10680 (2003).

[2] T.R. Dyke, K.M. Mack, and J.S. Muenter, J. Chem. Phys. **66**, 498 (1977).

[3] L.H. Coudert, F.J. Lovas, R.D. Suenram, and J.T. Hougen, J. Chem. Phys. **87**, 6290 (1987).

[4] J.A. Odutola, T.A. Hu, D. Prinslow, S.E. O'dell, and T.R. Dyke, J. Chem. Phys. **88**, 5352 (1988).

[5] T.A. Hu and T.R. Dyke, J. Chem. Phys. **91**, 7348 (1989).

[6] L. Martinache, S. Jans-bürli, B. Vogelsanger, W. Kresa, and A. Bauder, Chem. Phys. Lett. **149**, 424 (1988).

[7] E. Zwart, J.J.T. Meulen, and W.L. Meerts, Chem. Phys. Lett. **166**, (1990).

[8] E. Zwart, J.J. Ter Meulen, W. Leo Meerts, and L.H. Coudert, Journal of Molecular Spectroscopy **147**, 27 (1991).

[9] M.Yu. Tretyakov, E.A. Serov, M.A. Koshelev, V.V. Parshin, and A.F. Krupnov, Phys. Rev. Lett. **110**, 093001 (2013).

[10] Y. Scribano, N. Goldman, R.J. Saykally, and C. Leforestier, J. Phys. Chem. A **110**, 5411 (2006).

[11] M.Yu. Tretyakov, T.A. Galanina, A.O. Koroleva, D.S. Makarov, D.N. Chistikov, A.A. Finenko, and A.A. Vigasin, Journal of Quantitative Spectroscopy and Radiative Transfer **333**, 109319 (2025).

[12] H. Fleurbaey, S. Kassi, and A. Campargue, Phys. Chem. Chem. Phys. **26**, 21974 (2024).

[13] E. Vogt, I. Simkó, A.G. Császár, and H.G. Kjaergaard, J. Phys. Chem. A **127**, 9409 (2023).

[14] K.K. Lehmann and A.M. Smith, J. Chem. Phys. **93**, 6140 (1990).

[15] I.E. Gordon, L.S. Rothman, R.J. Hargreaves, R. Hashemi, E.V. Karlovets, F.M. Skinner, E.K. Conway, C. Hill, R.V. Kochanov, Y. Tan, P. Wcisło, A.A. Finenko, K. Nelson, P.F. Bernath, M. Birk, V. Boudon, A. Campargue, K.V. Chance, A. Coustenis, B.J. Drouin, J. –M. Flaud, R.R. Gamache, J.T. Hodges, D. Jacquemart, E.J. Mlawer, A.V. Nikitin, V.I. Perevalov, M. Rotger, J. Tennyson, G.C. Toon, H. Tran, V.G. Tyuterev, E.M. Adkins, A. Baker, A. Barbe, E. Canè, A.G. Császár, A. Dudaryonok, O. Egorov, A.J. Fleisher, H. Fleurbaey, A. Foltynowicz, T. Furtenbacher, J.J. Harrison, J.-M. Hartmann, V.-M. Horneman, X. Huang, T. Karman, J. Karns, S. Kassi, I. Kleiner, V. Kofman, F. Kwabia-Tchana, N.N. Lavrentieva, T.J. Lee, D.A.

Long, A.A. Lukashevskaya, O.M. Lyulin, V.Yu. Makhnev, W. Matt, S.T. Massie, M. Melosso, S.N. Mikhailenko, D. Mondelain, H.S.P. Müller, O.V. Naumenko, A. Perrin, O.L. Polyansky, E. Raddaoui, P.L. Raston, Z.D. Reed, M. Rey, C. Richard, R. Tóbiás, I. Sadiek, D.W. Schwenke, E. Starikova, K. Sung, F. Tamassia, S.A. Tashkun, J. Vander Auwera, I.A. Vasilenko, A.A. Vigasin, G.L. Villanueva, B. Vispoel, G. Wagner, A. Yachmenev, and S.N. Yurchenko, J. Quant. Spectrosc. Radiat. Transf. **277**, 107949 (2022).

[16] M. Herman, R. Georges, M. Hepp, and D. Hurtmans, International Reviews in Physical Chemistry **19**, 277 (2000).

[17] S.A. Nizkorodov, M. Ziemkiewicz, D.J. Nesbitt, and A.E.W. Knight, J Chem Phys **122**, 194316 (2005).

[18] T. Vanfleteren, T. Földes, and M. Herman, Chem. Phys. Lett. **627**, 36 (2015).

[19] T. Vanfleteren, T. Földes, M. Herman, J. Liévin, J. Loreau, and L.H. Coudert, J. Chem. Phys. **147**, 014302 (2017).

[20] K. Didriche and T. Földes, J. Chem. Phys. **138**, 104307 (2013).

[21] A.S. Bogomolov, R. Glorieux, M. Herman, T. Corbo, S. Collignon, B.M. Hays, D. Lederer, N. Moazzen-Ahmadi, A. Libert, B. Tomasetti, J. Fréreux, and C. Lauzin, Molecular Physics **123**, e2413417 (2024).

[22] D.F. Plusquellic, O. Votava, and D.J. Nesbitt, J. Chem. Phys. **101**, 6356 (1994).

[23] O. Votava, D.F. Plusquellic, T.L. Myers, and D.J. Nesbitt, J. Chem. Phys. **112**, 7449 (2000).

[24] O. Votava, S.R. Mackenzie, and D.J. Nesbitt, J. Chem. Phys. **120**, 8443 (2004).

[25] Q. Liu, J. Wang, Y. Zhou, and D. Xie, Current Chinese Science **2**, 325 (2022).

[26] R.C. Cohen, K.L. Busarow, K.B. Laughlin, G.A. Blake, M. Havenith, Y.T. Lee, and R.J. Saykally, J. Chem. Phys. **89**, 4494 (1988).

[27] G.T. Fraser, F.J. Lovas, R.D. Suenram, and K. Matsumura, J. Mol. Spectrosc. **144**, 97 (1990).

[28] S. Suzuki, R.E. Bumgarner, P.A. Stockman, P.G. Green, and G.A. Blake, J. Chem. Phys. **94**, 824 (1991).

[29] E. Zwart and W.L. Meerts, Chemical Physics **151**, 407 (1991).

[30] S. Li, R. Zheng, Y. Zhu, and C. Duan, Journal of Molecular Spectroscopy **272**, 27 (2012).

[31] J.T. Stewart and B.J. McCall, Journal of Molecular Spectroscopy **282**, 34 (2012).

[32] Xiang L., Yun L., Tian-Xin Z., and Chuan-Xi D., rhhzgw **72**, 013401 (2023).

[33] R. Glorieux, A.J. Barclay, C. Lauzin, A.R.W. McKellar, and N. Moazzen-Ahmadi, Mol. Phys. **122**, e2259012 (2024).

[34] M. Herman, T. Földes, K. Didriche, C. Lauzin, and T. Vanfleteren, Int. Rev. Phys. Chem. **35**, 243 (2016).

[35] A.S. Bogomolov, A. Roucou, R. Bejjani, M. Herman, N. Moazzen-Ahmadi, and C. Lauzin, Chem. Phys. Lett. **774**, 138606 (2021).

[36] C.M. Western, J. Quant. Spectrosc. Radiat. Transf. **186**, 221 (2017).

[37] J.M. Brown, J.T. Hougen, K.-P. Huber, J.W.C. Johns, I. Kopp, H. Lefebvre-Brion, A.J. Merer, D.A. Ramsay, J. Rostas, and R.N. Zare, Journal of Molecular Spectroscopy **55**, 500 (1975).

[38] A.R.W. McKellar and B.E. Billinghurst, Journal of Molecular Spectroscopy **383**, 111563 (2022).

[39] N.F. Zobov, R.I. Ovsannikov, S.V. Shirin, O.L. Polyansky, J. Tennyson, A. Janka, and P.F. Bernath, Journal of Molecular Spectroscopy **240**, 112 (2006).

[40] A.D. Bykov, O.V. Naumenko, E.R. Polovtseva, S.-M. Hu, and A.-W. Liu, Journal of Quantitative Spectroscopy and Radiative Transfer **111**, 2197 (2010).

[41] J. Tennyson, P.F. Bernath, L.R. Brown, A. Campargue, A.G. Császár, L. Daumont, R.R. Gamache, J.T. Hodges, O.V. Naumenko, O.L. Polyansky, L.S. Rothman, A.C. Vandaele, N.F. Zobov, N. Dénes, A.Z. Fazliev, T. Furtenbacher, I.E. Gordon, S.-M. Hu, T. Szidarovszky, and I.A. Vasilenko, Journal of Quantitative Spectroscopy and Radiative Transfer **142**, 93 (2014).

[42] S. Wang, S. He, L. Dai, E. Feng, and W. Huang, J. Chem. Phys. **142**, 224307 (2015).

[43] D. Hou, Y.-T. Ma, X.-L. Zhang, and H. Li, J. Chem. Phys. **144**, 014301 (2016).